Large-scale synthesis and photoluminescence of cobalt tungstate nanowires

Cuiling Zhang,[1,2] Donglin Guo,[1] Chenguo Hu,[1,*] Yanxue Chen,[3] Hong Liu,[3] Hulin Zhang,[1] and Xue Wang[1]

[1]*Department of Applied Physics, Chongqing University, Chongqing 400044, People's Republic of China*

[2]*School of Computer Science and Information Engineering, Chongqing Technology and Business University, Chongqing 400067, People's Republic of China*

[3]*State Key Laboratory of Crystal Materials, School of Physics, Shandong University, Jinan 250100, People's Republic of China*

(Received 16 August 2012; revised manuscript received 2 December 2012; published 18 January 2013)

Single-crystalline wolframite-type monoclinic structure cobalt tungstate ($CoWO_4$) nanowires were obtained by a solvothermal method at 180 °C for 24 h with a width of 20 nm and length of 200 to 400 nm. Besides the strong blue-green light emission at 10–250 K, we found much stronger and broader near-infrared emission ranging from 700–1000 nm at about 300 K under the excitation wavelength of 325 nm. The emission and the dependence of emission intensity on temperature are discussed by introducing the effect of Co vacancies. This near-infrared emission material might have potential applications in infrared detection or stealth technology.

DOI: 10.1103/PhysRevB.87.035416 PACS number(s): 78.55.Hx, 78.67.Uh, 42.70.Km

I. INTRODUCTION

Tungstates with large radii of bivalent cations (e.g., Ca, Ba, Pb, and Sr) surrounded by four oxygen atoms tend to form a scheelite-type tetragonal structure, while small cationic radii (e.g., Fe, Mn, Co, Ni, Mg, and Zn) surrounded by six oxygen atoms are in favor of forming a wolframite-type monoclinic structure. These materials, due to their excellent optical properties that form the basis of their wide applications as phosphors, laser crystals, and scintillation detectors, have been extensively studied for a long time.[1–3] Cobalt tungstate ($CoWO_4$), originally well-known for antiknock and pigment additives,[4,5] can also be applied to new fields because of its attractive catalytic activity,[6] microwave dielectric property,[7] and photoelectricity in the photovoltaic electrochemical cell.[8] Thus, the synthesis of well-crystallized nanostructure $CoWO_4$ crystallites with controllable size and shape has recently drawn increasing attention. Although several techniques for the preparation of $CoWO_4$ have been developed, such as spray pyrolysis,[9] the molten salt method,[10] and hydrothermal methods,[11,12] the products are mainly particlelike nanocrystals[9–11] or short nanorods.[3,12] It is a great challenge to prepare $CoWO_4$ nanowires on a larger scale. In addition, a number of studies of scheelite-type tungstates focus on the luminescent properties including the dependence of emission intensity and decay time on temperature and the influence of the Jahn–Teller (J-T) effect on the emission spectrum of the scheelite tungstate family, such as $PbWO_4$, $CaWO_4$, $BaWO_4$, and $SrWO_4$, which are based on the radiative transition within the tetrahedral $(WO_4)^{2-}$ group.[13,14] Meanwhile, other research on wolframite-type tungstates in the $(WO_6)^{2-}$ group (with a different luminescence center) mainly focuses on the emission spectrum at room temperature in the range of the visible region.[15–23] $ZnWO_4$ and $CdWO_4$ thin films showed a similar broad blue-green emission band centered at 495 nm,[16] and near-infrared (NIR) emission could only be found in their imperfect structure (Cr^{3+}:$ZnWO_4$ and Co:$CdWO_4$).[18,19] Therefore, it is necessary to perform investigations systematically, including the dependence of emission intensity and fluorescence quenching on temperature and to get a complete picture of the processes of light emission. In this case, it is very interesting to explore the dependence of luminescence on temperature and the phenomenon of the (NIR) emission in pure wolframite-type monoclinic crystals with this nanostructure.

Motivated by these purposes, we undertook the study of the synthesis, the structural and optical properties of wolframite-type monoclinic $CoWO_4$ nanowires. The ultraviolet (UV)-visible reflection spectrum and room-temperature and low-temperature photoluminescence (PL) spectra of $CoWO_4$ nanowires were measured. Structural information and the PL mechanism were obtained by analyzing experimental data within the framework of theoretical calculations.

II. EXPERIMENTAL CONDITIONS

We present a facile and general approach to prepare $CoWO_4$ nanowires. Typically, 0.1 M $CoCl_2{\cdot}6H_2O$ and 0.1 M Na_2WO_4 $2H_2O$ were placed into a Teflon vessel with 16 mL of absolute ethanol and 4 mL of ammonia (pH = 10). The vessel was heated at 180 °C for 24 h in a furnace. After the vessel cooled to room temperature, the blue solid products were collected, washed several times using deionized water and ethanol, and dried at 60 °C for 1 h.

Transmission electron microscopy (TEM) with the JEOL-4000EX was used to characterize the morphology and size of the synthesized samples. The crystal phase and chemical composition were characterized by an x-ray diffractometer (BDX3200) equipped with Cu Ka radiation ($\lambda = 1.5418$ Å) at a 2° per minute scanning speed in the 2θ range from 30° to 70° and energy dispersive spectrum (EDS). Electronic properties of the $CoWO_4$ tungstates were studied on an ESCALab MKII x-ray photoelectron spectrometer, using a nonmonochromatized Mg Ka x-ray as the excitation source. To examine the optical band gap of the samples, we measured the reflectance of a film made of the $CoWO_4$ nanowires on a quartz slice with a UV-Vis-NIR spectrophotometer (Hitachi U-4100) under a normal incidence of light. The PL spectra were measured on a glass slice under the irradiation of a 6-mW HeCd laser at a wavelength of 325 nm from 10–300 K.

III. RESULTS AND DISCUSSION

A. Characterization of cobalt tungstate nanowires

The x-ray diffraction (XRD) pattern in Fig. 1(a) indicates high crystallization of the sample. All diffraction peaks are readily indexed to a pure wolframite-type monoclinic phase [P2/a (13)] of $CoWO_4$, with lattice constants of $a = 0.495$ nm, $b = 0.568$ nm, $c = 0.466$ nm, and $\alpha = \gamma = \beta = 90.0°$, which

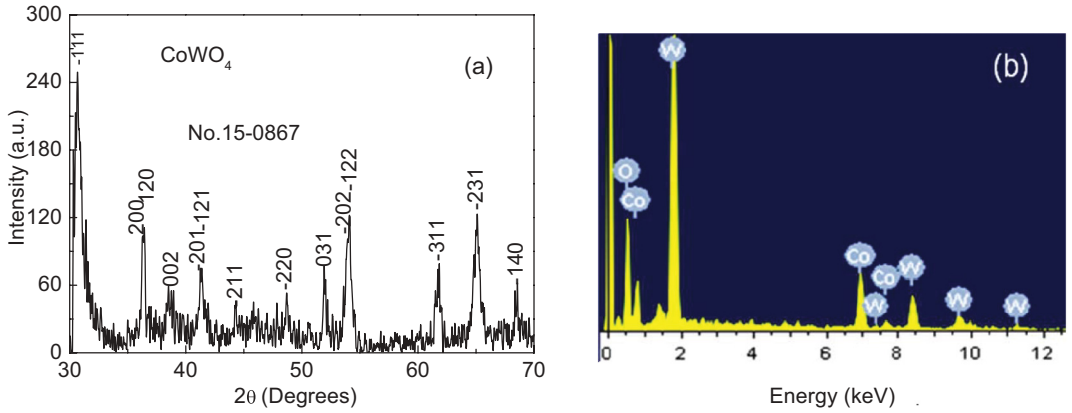

FIG. 1. (Color online) The structure and composition characterization of the $CoWO_4$ sample: XRD pattern (a) and EDS (b).

match well with the standard XRD pattern for $CoWO_4$ (JCPDS Card No. 15-0867). The EDS pattern in Fig. 1(b) indicates that the elements in the sample are Co, W, and O. The TEM image in Fig. 2(a) exhibits the shape of $CoWO_4$ nanowires 200–400 nm in length and 20 nm in width. Therefore, the $CoWO_4$ nanowires have a large specific surface area and high aspect ratio, which is typical of optical nanomaterials. The high-resolution TEM (HRTEM) image, fast Fourier transform (FFT) pattern, and the inset in Fig. 2(b) demonstrate a single-crystal structure of the rod with the growth direction along [011].

To work out the energy state structure, Fig. 3 shows the x-ray photoelectron spectroscopy (XPS) spectrum of $CoWO_4$ nanowires. For the cobalt tungstate, all the spectral features, except the C 1s level, are attributed to the constituent element core levels or Auger lines. The existence of the C 1s line on the survey XPS spectrum [Fig. 3(a)] owes a good deal to the hydrocarbons adsorbed on the $CoWO_4$ nanostructure surface, whereas the intensities of the C 1s core-level lines are rather low for the cobalt tungstate. The high-resolution XPS of W 4f, O 1s, and Co 2p are shown in Figs. 3(b)–3(d), respectively. Table I shows the peak positions and the corresponding core levels. The spectrum of the W exhibits a main peak at 35.15 eV as well as a peak at 37.20 eV, which is assigned to a simple spin-doublet W $4f_{7/2}$ state and W $5p_3$, respectively. This indicates that the oxidation state of tungsten is $+6$. The core-level binding energies of the XPS W 4f and O 1s are slightly less than those in other representative scheelite- and wolframite-type tungsten-bearing materials,[12,24] such as $FeWO_4$, $CoWO_4$, and Na_2WO_4. The fitted XPS spectrum for Co exhibits peaks at 781.01 ($2p_{3/2}$), 786.11 (shake-up satellite), 796.94 ($2p_{1/2}$), and 802.56 eV (satellite peak). The difference in peak 1 and peak 3 is about 15.8 eV. Compared with other XPS data, we found that cobalt atoms in the $CoWO_4$ nanowires are in the formal valence $+2$. Quantitative analysis shows that the molar ratio of Co to O to W is about 14:69:17, which is approximately in agreement with the nominal composition of $CoWO_4$. The composition of the $CoWO_4$ nanowires, compared with a stoichiometric one, is abundant in Co cationic vacancies (V_{Co}). Therefore, the negatively charged cationic vacancies could capture the positive charges so as to keep it neutral. A possible process was expressed as follows:

$$2Co_{Co}^{2+} + \tfrac{1}{2}O_2(g) \Leftrightarrow 2Co_{Co}^{2+} + 2h^{\bullet} + V_{Co}^{''2-} + O_O(ad) \Leftrightarrow 2Co_{Co}^{3+} + V_{Co}^{''2-} + O_O, \quad (1)$$

where Co_{Co}^{2+}, $O_2(g)$, $O_O(ad)$, $h^{\bullet}$, $V_{Co}^{''2-}$, O_O and Co_{Co}^{3+} are, respectively, the Co cation in the cobalt position, oxygen gas, adsorbed oxygen atom, hole, negatively charged Co^{2-} cationic vacancy, oxygen atom at oxygenic lattice site, and Co^{3+} cation at the cobaltic lattice site. So, there are a large number of Co^{3+} cations distributed in the cobalt tungstate lattice due to the Co cationic vacancies. Consequently, coupling of Co^{3+} to cation vacancy can provide excess electrons in the conduction band similar to the $PbWO_4$:Mo, La sample.[25] Co^{3+} ions as donor impurities can efficiently capture and inactivate excess free electrons in the deep-trap defect sites in the lattice.

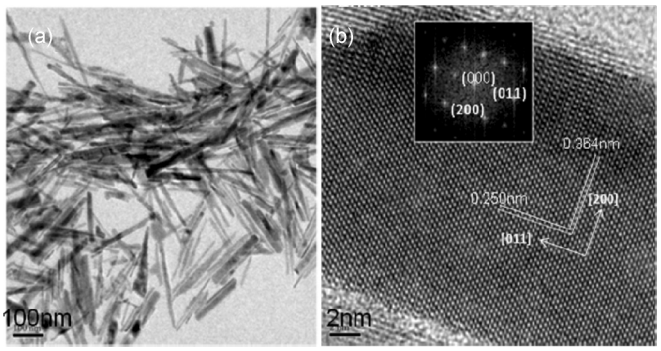

FIG. 2. (a) TEM images of the $CoWO_4$ nanowires, (b) HRTEM image of an individual $CoWO_4$ nanowire and the corresponding FFT pattern (inset).

B. Optical properties

The optical properties were investigated via the diffuse spectrum and PL spectrum. The optical energy gap (Eg) of $CoWO_4$ nanowires can be obtained from the Kubelka–Munk (K-M) function, which can be expressed by the following:[26]

$$\alpha = S(1-R)^2/2R, \quad (2)$$

where, α, R, and S are absorbance, reflectivity and scattering factor, respectively. S can be taken as a constant because an ideal diffuse reflection can be assumed when the size of individual nanowires is much less than the thickness (about

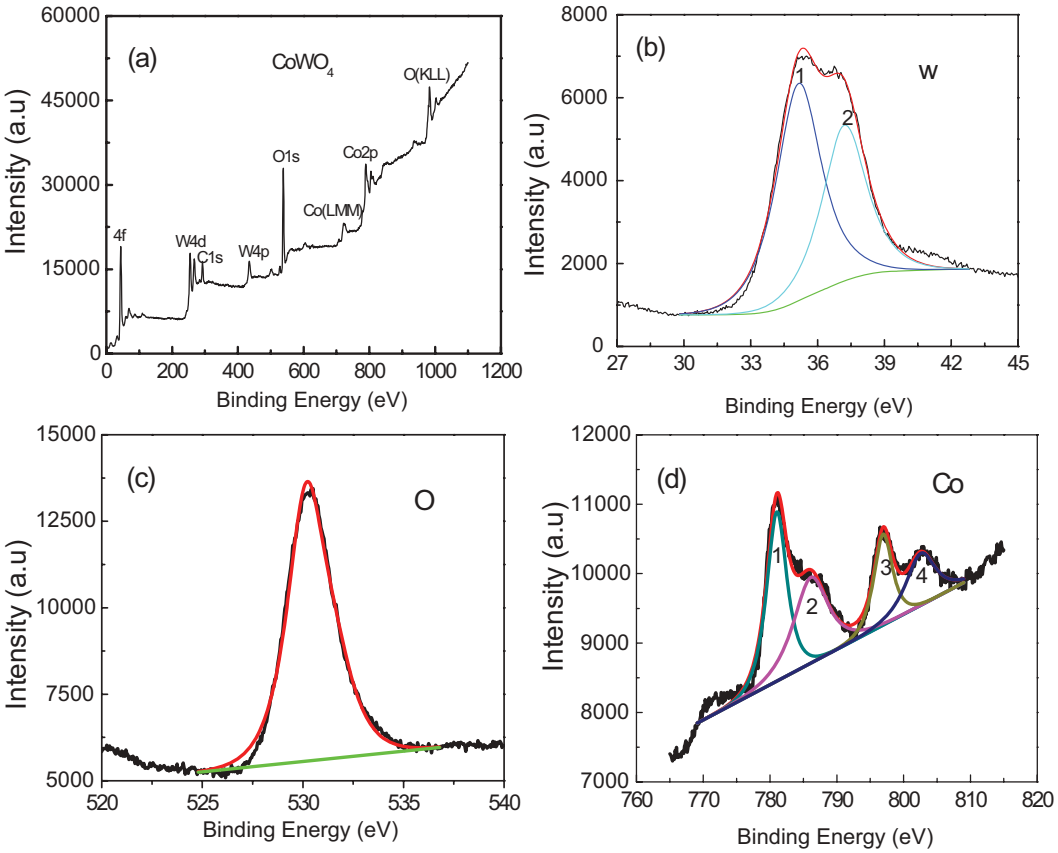

FIG. 3. (Color online) XPS spectra of $CoWO_4$ products: a typical survey spectrum (a), W 4f core level (b), O 1s core level (c), and Co core level (d).

1 mm) of the $CoWO_4$ nanowire film. The K-M function can be plotted vs photon energy, as is shown in Fig. 4. There are more than five steps in the spectrum of the K-M function. The steps 1, 2, and 3 are faint oscillation absorption in the NIR region, and the stronger absorption starting at steps 4 and 5 may result from electron transition from the valence band to conduction band. The band gap (or more precisely, the optical band gap) calculated by extrapolation of linear part of the curve starting from step 4 and peak 5 to zero, $Eg = 2.24$, 2.38 eV, which is somewhat different from the previous report of 1.8 and 2.68 eV.[27] Bharati pointed out that the band gap of bulk $CoWO_4$ is 2.8 eV.[28] The decreased band gap of the $CoWO_4$ nanowires with respect to bulk or nanoparticle $CoWO_4$ is a result of wave function overlapping due to the domination of internal stress coming from cobalt vacancies and surface relaxation from the large ratio of surface area to volume.

It is well known that tungstates are a good candidate for PL materials; however, the light-emitting property of the tungstate crystal is greatly influenced by temperature, and it is likely to have fluorescence quenching at room temperature. To explore the optical property of the $CoWO_4$ nanowires, we carried out PL spectra under the HeCd laser irradiation at different temperatures, as shown in Fig. 5. As there were no noticeable changes in the PL spectra of tungstates with wolframite structure under different excitation energy,[23] we, therefore, took PL spectrum measurements under the excitation wavelength of 325 nm. From Fig. 5(a), we can see a strong blue-green peak around 495 nm with a shoulder at 530 nm and a wide emission band within 750–990 nm of the overlap of spectral lines at temperature $\leqslant$250 K. The blue-green emission spectrum can be separated into two peaks (495 and 530 nm), indicating that it consists of more than one emission band. A similar broad emission spectrum was observed at a larger region from 350–550 nm in the scheelite tungstate family, including $PbWO_4$, $CaWO_4$, $BaWO_4$, and $SrWO_4$,[14] while the broad emission band of $ZnWO_4$ and $CdWO_4$ films with same structure centered at 495 nm (2.51 eV) and about 540 nm (2.30 eV).[16] So, $CoWO_4$ has the same luminescence center $(WO_6)^{6-}$ as that of $CdWO_4$ and $ZnWO_4$ because the PL spectra at the visible region are

TABLE I. Values of the XPS W, O, and Co core-level binding energies.

Element	O	W			Co		
State	1s	4$f_{7/2}$	5p_3	2$p_{3/2}$	2$p_{3/2}$ (Sat)	2$p_{1/2}$	2$p_{1/2}$ (Sat)
Binging energy (eV)	530.25	35.15	370.20	781.02	786.11	796.94	802.56

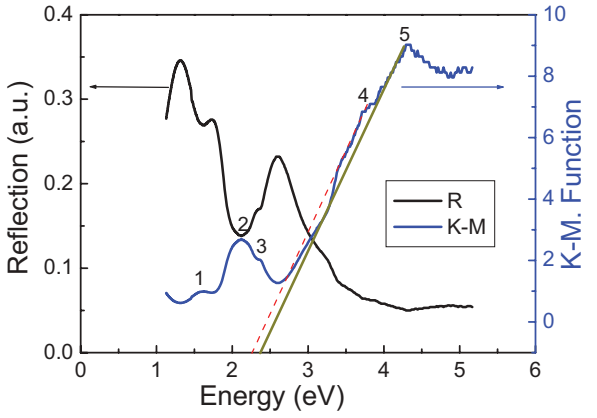

FIG. 4. (Color online) The uv-visible reflection spectrum and K-M function of $CoWO_4$ nanowires.

similar. The emission band shape was numerically calculated by the semiclassical approach using Monte Carlo integration, and the result showed that the emission was broadened or split by J-T effects caused by the antisymmetric charge density.[25] Figure 5(b) displays the plots of intensity of the spectra vs temperature. The intensity of blue-green emission of $CoWO_4$ below 200 K is similar to the emission intensity of $PbWO_4$ below 170 K (for details of the evaluation, see Refs. 13 and 14). There are four noticeable effects of temperature on the luminescence of $CoWO_4$: (1) the luminescence spectra are very similar at different temperatures, (2) a decrease of the visible emission intensity, with an increase in temperature firstly, then increase abruptly and decrease finally, (3) a slight redshift of the visible emission, and (4) emission intensity of the infrared remains constant at low temperature, with an increase exponentially after the temperature reaches 200 K. Therefore, $CoWO_4$ nanowires have a visible emission at low temperature and a strong infrared PL at room temperature.

To explain the PL spectrum, we constructed a perfect structure and a small supercell crystal structure with a cobalt vacancy [Fig. 6(a)] and then calculated the band structure of the perfect $CoWO_4$ crystal [Fig. 6(b)], its electron density of states (DOS), and partial DOS [PDOS; Figs. 6(c) and 6(d)] on the basis of density functional theory (DFT) by the pseudopotential plane-wave method. All the calculations and the Brillouin zone integration are performed with W $5s2\ 5p6\ 5d4\ 6s2$, Co $3d7\ 4s2$, and O $2s2\ 2p6$ treated as valence electrons. Figure 6(a) shows that the wolframite supercell $CoWO_4$ structure with cobalt vacancy has the WO_6 octahedral complex with asymmetric shape, which has short, medium, and long W-O distances. The octahedral crystal field splits the degenerate spatial orbital into five discrete orbitals, a lower triplet of t_{2g} symmetry (the d_{xy}, d_{xz}, and d_{yz} orbits) and an upper doublet of e_g symmetry (the $d_{x^2-y^2}$ and d_{z^2} orbits). Their energy separation 10 Dq is about 2 eV.[29,30] The zero level is set as the Fermi level in the band structure in Fig. 6(b). The positive level corresponds to the conduction band and negative level to the valence band. We can see that the top of the valence band and the bottom of the conduction band are located at different k points, indicating the indirect band structure. Such results give strong support to the above experiment that the electron transition from the valence band to the conduction band has two absorption peaks 4 and 5. The band gap is 1.0 eV, which is underestimated in comparison with the experimental value of 2.24 eV due to the limitations of the generalized gradient approximation (GGA). Although the band gap calculated by the GGA is not accurate, the electronic states near the top of valence and bottom of conduction band can be well evaluated. Figure 6(c) shows that DOS of the pure and defect structure are similar. A clear distinction can be seen at the edges of the valence band and the conduction band. An impurity level present in the band gap at the top of the valance band and the edge of conduction band moves about 0.04 eV to lower energy. Figure 6(d) shows that three parts of the conduction band mainly associate with the Co $3d$, O $2p$, and W $5d$ states in pure $CoWO_4$. W $5d$ states have significant influence on the conduction-band higher-energy region. The Co $3d$ and O $2p$ states mainly contribute to the two lower conduction-band regions. However, the maximum contributions of the O $2p$ states occur in the whole valence-band region of the pure $CoWO_4$. The results are consistent with previous studies on the electronic properties of $CoWO_4$.[31] Figure 6(e) indicates that the impure level is mainly attributed to hybridization of O $2p$ states with Co $3d$ states. Due to possible oscillation of the cobalt charge state between $2+$ and $3+$ near a cobalt vacancy

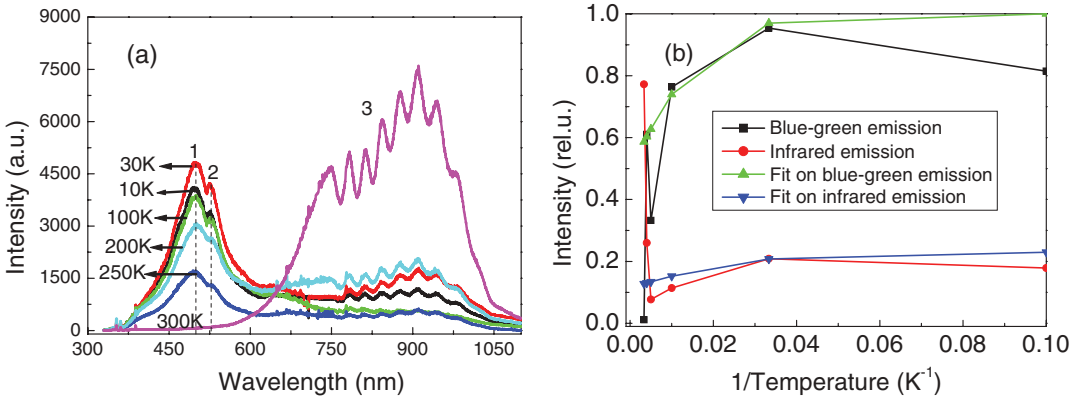

FIG. 5. (Color online) (a) The room-temperature and low-temperature emission spectrum of $CoWO_4$ nanowires at the excitation wavelength 325 nm; (b) variation of emission intensity with the temperature of $CoWO_4$ nanowires and the corresponding fit curve.

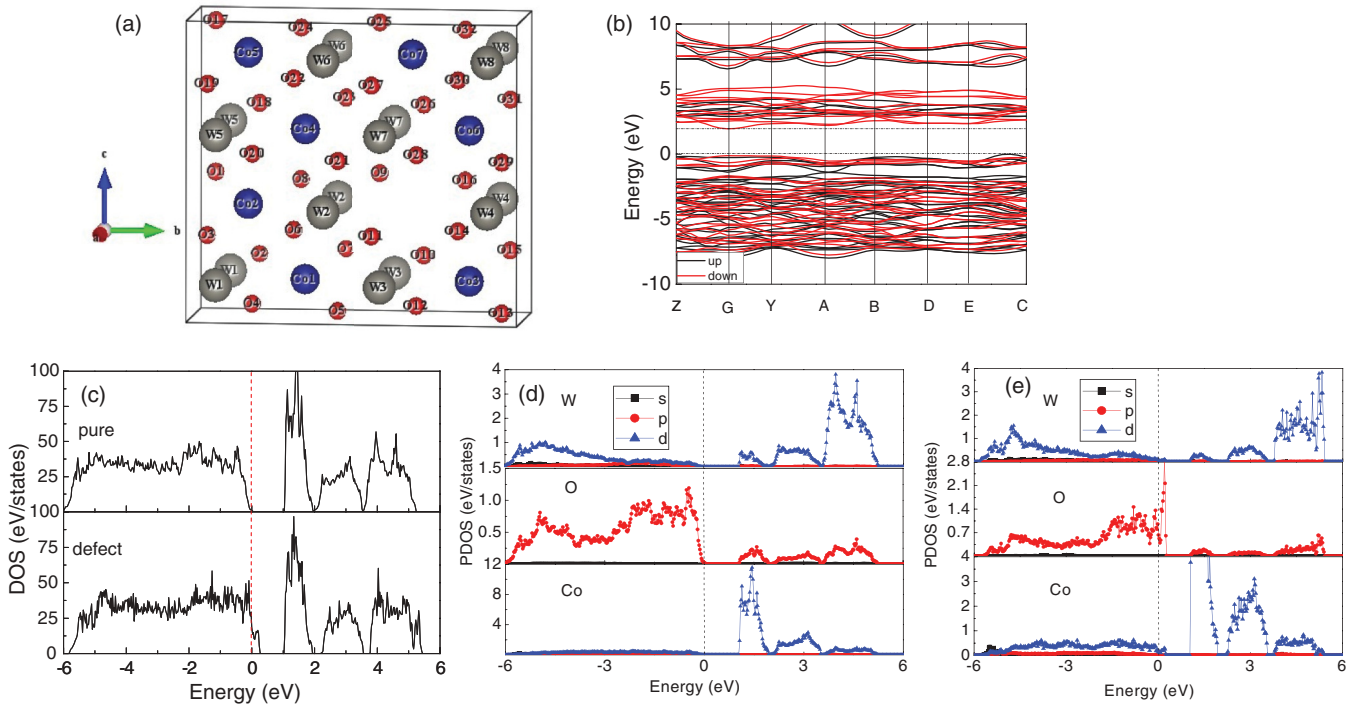

FIG. 6. (Color online) (a) The supercell of wolframite $CoWO_4$ with Co vacancy; (b) the band structure of $CoWO_4$ nanocrystal; (c) the total DOS of pure $CoWO_4$ and $CoWO_4$ with defects, (d) the PDOS of pure $CoWO_4$, and (e) the PDOS of $CoWO_4$ with defects.

and participation of the Co^{2+} at the edges of the valence and conduction bands, $CoWO_4$ remains very much trivalent ions. Therefore, electron state hybridization of the O $2p$ states, W^{6+} $5d$, Co^{3+} $3d$, and Co^{2+} $3d$ is expected, which has an important influence on the electronic traps.

From the above calculations and experiment results, we believe that the blue-green emission is a result of electronic transition from W to O. According to molecular-orbital calculations, the levels are divided into the ground state $^1A_{1g}$ and the excited state $^3T_{1g}$, $^1T_{1g}$, $^3T_{1u}$, $^1T_{1u}$ as is shown in Fig. 7(a). In this case, the highest occupied state with e_g symmetry of W $5d$ is associated with the $2p$ orbital of oxygen, and the excited state consists of an electron at the W $5d$ orbital with t_{2g} symmetry of

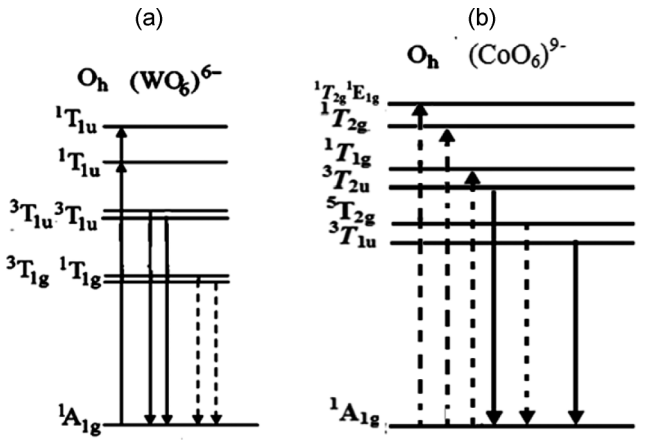

FIG. 7. The schematic energy level diagrams for the visible luminescence processes (a) and the infrared luminescence processes (b) in the $CoWO_4$ nanowires.

two closely lying triplet states $^3T_{1u}$. When the sample is excited at the wavelength of 325 nm, electron transition starts from two close $^3T_{1u}$ levels to the $^1A_{1g}$ level as is shown in Fig. 7(a). Thus, the most possible emission on 495 nm is obtained. The spin-forbidden transitions from T_{1g} to $^1A_{1g}$ are partly allowed by spin-orbit coupling, and this would contribute to the luminescence on the longer wavelength of 530 nm. However, according to the calculations suggested by Ref. 32, the intensity relation between the peaks (about 495 nm) depends on the values of the J-T coupling constants, while the intensity of the low-energy peak (about 530 nm) is not affected by a change of coupling parameters in $PbWO_4$ due to the only partially allowed transition. In this case the low-energy peak of 530 nm was attributed to the radiative transition of the tungstate group with oxygen ion vacancy in scheelite-type $CaWO_4$ and $PbWO_4$.[13,32] So, there is no clear conclusion with regard to the low-energy peak of 530 nm. Meanwhile, oxygen vacancy-related centers should not be of concern in the $CoWO_4$ crystal, because Co^{3+} impurity effectively prevents the creation of oxygen vacancies.[33] This result agrees with Lou *et al.*,[16] suggesting that oxygen vacancies were not related to the emission of $ZnWO_4$ and $CdWO_4$, but in the $CoWO_4$ crystal, where a lot of cobalt vacancies would distort the structure configuration. In this case we are prone to suggest that the emission band should be related to the WO_6 group near with cobalt vacancies [as sketched in Fig. 6(a)]. A possible increase in the lowest-energy peak intensity could be expected by perturbation of WO_6 octahedra since the high concentration of Co vacancies induce the higher population of W $5d$ states in lower-energy level T_{1g}. It is proved by the calculations of DOS of $CoWO_4$ with cobalt vacancy that the DOS at the lower-energy region increases.

According to the Vashni equation,

$$E_g(T) = E_g(0) - \alpha T^2/(T+\beta), \quad (3)$$

where $E_g(0)$ is the band gap at 0 K and α and β are fitting parameters. With an increase in temperature, the decrease in band gap results in a slight redshift of the PL peaks. So, emission peak 2 has a slight redshift when the temperature rises, which proves the above scenario about emission.

The emission intensity of $CoWO_4$ [Fig. 5(b)] vs temperature complies with the classical exponential form

$$I = I_0/(1 + e^{-\Delta E/kT}). \quad (4)$$

The extra vibration energy to nonradiative transition in the configuration coordinate chart $\Delta E = 11.8$ and 6.8 meV for blue-green emission and infrared emission, respectively. The best-fit curves for the intensity are shown in Fig. 5(b). However, obvious disagreement above 200 K for blue-green emission is observed, and the decrease in intensity is much faster than that of the fitting line. When discussed the temperature dependence (TD) of $PbWO_4$ on the emission intensity the thermal disintegration of excitonic state (i.e., not simple intracenter thermal quenching) is proposed.[13,14] The local photocarrier energy in the PL center increases with an increase in temperature. When T is up to 200 K, the increased activation energy of the exciton induces the disintegration of the exciton to produce free electrons and holes. Some free carriers can experience radiative recombination at the same emission center afterwards, while others can experience the electron transfer quenching for strong local d-d interaction of Co 3d and W 5d that occupy the bottom of the conduction band and the top of the valence band. The combined interaction of temperature quenching and transfer quenching of free electrons and holes coming from the disintegration of excitons leads to the decline of intensity. It is worth stressing that the peaks of thermostimulated luminescence (TSL) intensity spectra are observed at about 110 and 190 K for $PbWO_4$ and at 160 K for $CaWO_4$.[14] Analogously, $CoWO_4$ at low temperature stores some energy in the luminescence center under the irradiation, which can be released by thermal energy at higher temperature. In the case of $CoWO_4$, a remarkable enhancement on the emission strength is observed when $T =$ 250 K for a TSL effect. Therefore, when $T = 300$ K, the fluorescence quenches as a result of the synergistic interaction of temperature quenching and electron transfer quenching.

The origin of the NIR luminescence remains unclear in $CoWO_4$. Previous investigations have demonstrated that the NIR luminescence is caused by the defect in tungstate crystals. Kushnirenko *et al.*[34] have investigated luminescence properties of $CdWO_4$-Ag and $CdWO_4$-W crystals and ascribed the infrared emission to the radiative transition in the tungstate group that lacks one oxygen ion. Strong emission peaks from 600 to 1000 nm in Cr^{3+}:$ZnWO_4$ crystal due to V_{Zn} near Cr^{3+} were detected, and only one strong emission peak was found in the visible region when there were no V_{Zn} near Cr^{3+}.[19] The role of point defects was investigated in $ZnWO_4$ crystal, and it was discovered that the V_O and V_{Zn} defects have significantly different influence on the electronic transition spectrum. In the case of V_O, the number and oscillator strength of transitions in the 0- to 4.5-eV region decrease in comparison with the case of the perfect crystal. On the contrary, the number and oscillator strength of transition increase in the case of V_{Zn}.[35] Therefore, the emission spectrum of real $ZnWO_4$ crystal at these energies can mainly be ascribed to electronic transitions in Zn^{2+} and WO_6^{2-}, with zinc vacancies in the nearest surroundings. Speaking in more detail, cationic vacancies have significant influence on the emission of tungstates.

The infrared emission of $CoWO_4$ should be similar to $ZnWO_4$, and there are a large number of Co cation vacancies in both cases that lead to the existence of Co^{3+} in $CoWO_4$ nanowires. We then have a hypothesis on the infrared emission that the $V_{Co}{}^{2+}$ rather than $V_O{}^{2-}$ has a significant influence on the infrared emission. According to the former analysis, it is worth noticing that the Co^{3+} is considered at high concentration due to the coupling of cation vacancy to Co^{3+}. In view of the properties of local electron of narrow 3d bands, $CoWO_4$ carrier transport would involve carriers jumping from a Co^{2+} ion to a neighboring Co^{3+} ion. Due to possible oscillation of the cobalt charge state between 2+ and 3+ and participation of the Co^{2+} at the edges of the valence and conduction bands, many charge carriers are captured at discrete Co^{3+} sites. Co^{2+} and Co^{3+} present the order and disorder in the crystal, which is best for PL emission because the discontinuities in the potential can help the trapping of electrons and holes on the localized Co^{3+} levels. It is worth noting that the competitive processes in lattice traps and deep-level carrier capture that can efficiently suppress carrier lattice traps were demonstrated in La-doped $PbWO_4$.[36] Bharati and Singh[29] also presented the existence of Co^{3+} sites by the constant thermoelectric power below 750 K in $CoWO_4$ crystal. They found that the intrinsic conduction is weak, and the extrinsic conduction (dominated by Co^{3+}) increases exponentially with a temperature increase for the higher thermal activation energy at a temperature of 200–700 K.

As a good discrete PL center, Co^{3+} ion are surrounded by six oxygen atoms, and the octahedral crystal field splits the degenerate spatial orbital into five discrete orbitals, a lower triplet of t_{2g} symmetry and an upper doublet of e_g symmetry. It is known that the effective nuclear charge (Z_{eff}) of free Co^{3+} is about 7.25 eV, and this value is reduced by 15–20% until 5.8 eV in the crystalline environment. Consequently, Z_{eff} is at the region of 6.2–6.4 eV for the same group octahedral $(CoO_6)^{9-}$ in $RBaCo_2O_{5.5}$ for higher spin states and lower spin states.[37] So, the Z_{eff} is taken about 6.2 eV in $CoWO_4$ nanowires. According to the Tanabe–Sugano diagram of Co^{3+}, it can be deduced that the ground state is $^1A_{1g}$ and the lower-lying excited electron configuration associated with the metal d orbital contains some states, $^1T_{2g}\,{}^1E_{1g}$, $^1T_{2g}$, $^1T_{1g}$, $^3T_{2u}$, $^5T_{2g}$ and $^3T_{1u}$, in order of decreasing energy based on the ligand field theory.[37] From our analysis, such a schematic energy level diagram for the infrared luminescence processes in the $[CoO_6]^{9-}$ complex in the wolframite structure is shown in Fig. 7(b). It is generally accepted that the parity-forbidden electronic transitions ($^1A_{1g} \rightarrow {}^1T_{2g}\,{}^1E_{1g}$, $^1T_{2g}$, $^1T_{1g}$) are partially allowed by J-T distortion and distortion from cobalt vacancy of $CaWO_4$, which is a weak absorption, and the transitions from lower-lying triplets $^3T_{2u}$, $^5T_{2g}$, and $^3T_{1u}$ to $^1A_{1g}$ are responsible for the NIR radiative transitions. Radiative recombination with phonons emitted brings the emission spectra into a series of emission spectral lines, thus, we obtained an emission band in the NIR.

When $CoWO_4$ is under irradiation at a wavelength of 325 nm in the low-temperature region, carriers are excited to the higher levels of the $(CoO_6)^{9-}$, $(CoO_6)^{10-}$, and $(WO_6)^{6-}$ groups and then transfer to the lower ones of Co^{3+} by the disturbance of the nonradiative phonon. Some of them are a radioactive recombination in the center Co^{3+}, and others are a nonradioactive recombination. The transitions would contribute to the population of the lower levels, thereby increasing the intensity of the emission from those transitions. Earlier electron spin resonance studies on Mo-doped $PbWO_4$ crystals showed that the carriers captured by Mo depended on temperature.[33] Similar to Mo-doped $PbWO_4$ crystals, the capability of capturing carriers of Co^{3+} does not depend on temperature up to 30 K and then increases exponentially in the temperature range of 200–300 K and finally would disappear at higher temperature (higher than the temperature of thermal ionization of Co^{3+}). So, the infrared emission intensity is lower than that of the blue-green emission for its lower population due to the competitiveness of carrier capture in impurity (Co^{3+}) and lattice (WO_6). The infrared PL would have thermal quenching according to Eq. (4). The best-fit curve of thermal quenching shown in Fig. 5(b) is in disagreement with the experiment result at $T > 200$ K. The variation of intensity with temperature is similar to the rule of TD on blue-green emission for the same cause of the temperature quenching at $T < 200$ K. At $T > 200$ K, the carriers with large thermal activation have higher probability to realize the local *d-d* transition from captured center $(CoO_6)^{10-}$ and $(WO_6)^{6-}$ groups to $(CoO_6)^{9-}$ due to the strong interaction among these groups, especially the interaction of Co^{2+} with Co^{3+}. Thereby, photoproduced electrons and holes captured by Co^{3+} ions rapidly increase due to higher effective transition with larger thermal activation energy in the complexes. Radiative recombination of electrons and holes captured by Co^{3+} ions increase exponentially with an increase in temperature in spite of thermal quenching. Moreover, excitonic thermal disintegration and TSL can improve the intensity of infrared emission. For all the above reasons, the intensity increases with temperature at $T > 200$ K.

IV. CONCLUSIONS

Single-crystalline wolframite-type monoclinic structure cobalt tungstate nanowires 20 nm in width and 200 to 400 nm in length were obtained. The UV-visible spectrum showed that cobalt tungstate nanowires have two optical gaps (2.24 and 2.38 eV). The strong blue-green light emission at 10–200 K was found from PL spectra measured at the excitation wavelength of 325 nm. The blue-green emission at 495 and 530 nm are ascribed to electronic transition from two close $^3T_{1u}$ levels to $^1A_{1g}$ and from T_{1g} to $^1A_{1g}$ allowed partly from spin-orbit coupling, respectively. Co vacancies near $(WO_6)^{6-}$ octahedron raised the population of the lower-energy level T_{1g} and increased the emission intensity at 530 nm. The TD of emission intensity depended on the combined action of temperature quenching, the exciton thermal disintegration, carriers transfer quenching and TSL. Besides the strong blue-green light emission, we found much stronger and broader NIR emission ranging from 700–1000 nm at room temperature. The NIR emission could mainly be ascribed to the discrete PL center Co^{3+} ions nearby the Co cationic vacancy. The carriers captured by the $(CoO_6)^{10-}$ and $(WO_6)^{6-}$ groups had a higher probability to realize the local *d-d* transition to Co^{3+} under large thermal activation due to the strong interaction among these groups, especially the interaction of Co^{2+} with Co^{3+} at $T > 200$ K. The synergistic interaction of excitonic thermal disintegration, TSL, and the increase in photoinduced carriers captured by Co^{3+} ions led to the exponential increase in NIR emission intensity. This NIR emission material might have potential applications in infrared detection or stealth technology.

ACKNOWLEDGMENTS

This work is supported by the NSFCQ cstc2012jjB0006, NSFC 60976055, Project No. WLYJSBJRCTD201101 of the Innovative Talent Funds for 985 Project No. SRFDP 20110191110034, NSFDYS 50925205, and the Large-Scale Equipment Sharing Fund of Chongqing University.

*Corresponding author: hucg@cqu.edu.cn

[1] J. M. Cano-Torres, M. Rico, X. Han, M. D. Serrano, C. Cascales, C. Zaldo, V. Petrov, U. Griebner, X. Mateos, P. Koopmann, and C. Kränkel, Phys. Rev. B **84**, 174207 (2011).
[2] A. Vedda, F. Moretti, M. Fasoli, M. Nikl, and V. Laguta, Phys. Rev. B **80**, 045104 (2009).
[3] V. V. Laguta, M. Buryi, M. Nikl, J. Rosa, and S. Zazubovich, Phys. Rev. B **83**, 094123 (2011).
[4] R. C. Weast, *Handbook of Chemistry and Physics: A Ready-Reference Book of Chemical and Physical Data* (CRC Press, Boca Raton, 1983), p. 63.
[5] V. V. Eremenko and V. M. Naumenko, JETP Lett. **7**, 326 (1968).
[6] D. L. R. Thelma, C. M. Virginia, D. V. Manuel, and L. O. Alejandro, Int. J. Chem. React. Eng. **5**, A30 (2007).
[7] R. C. Pullar, S. Farrah, and N. M. C. N. Alford, J. Eur. Ceram. Soc. **27**, 1059 (2007).
[8] P. K. Pandey, N. S. Bhave, and R. B. Kharat, J. Mater. Sci. **42**, 7927 (2007).
[9] S. Thongtem, S. Wannapop, and T. Thongtem, Ceram. Int. **35**, 2087 (2009).
[10] Z. W. Song, J. F. Ma, H. Y. Sun, Y. Sun, J. R. Fang, Z. S. Liu, C. Gao, Y. Liu, and J. G. Zhao, Mater. Sci. Eng., B **163**, 62 (2009).
[11] S. J. Naik and A. V. Salker, Solid State Sci. **12**, 2065 (2010).
[12] X. C. Song, E. Yang, R. Ma, H. F. Chen, and Y. Zhao, J. Nanopart. Res. **10**, 709 (2008).
[13] V. Mürky, M. Niklz, E. Mihokováz, and K. Nitschz, J. Phys.: Condens. Matter. **9**, 249 (1997).
[14] M. Nikl, P. Bohacek, E. Mihokova, M. Kobayashi, M. Ishii, Y. Usuki, V. Babin, A. Stolovich, S. Zazubovich, and M. Bacci, J. Lumin. **87–89**, 6113 (2000).
[15] F. A. Kröger, *Some Aspects of the Luminescence of Solids* (Elsevier, New York, 1948).
[16] Z. D. Lou, J. H. Hao, and M. Cocivera, J. Lumin. **99**, 349 (2002).

[17] A. E. Ovechkin, V. D. Ryzhikov, G. Tamulatis, and A. Zukauskas, Phys. Status Solidi A **103**, 285 (1987).
[18] C. Yu, H. P. Xia, D. J. Wang, and H. B. Chen, Spectrosc. Spectral Anal. **33**, 2350 (2011).
[19] W. Chen, S. D. Xia, H. G. Tang, J. Q. Liu, J. C. Zang, and S. K. Wan, Acta Phys. Sin. **5**, 851 (1994).
[20] G. B. Beard, W. H. Kelly, and M. L. Mallory, J. Appl. Phys. **33**, 1728474 (1962).
[21] R. Grasser, A. Sharmann, and K. R. Strack, J. Lumin. **27**, 263 (1982).
[22] S. Chernov, L. Grigorjeva, D. Millers, and A. Watterich, Phys. Status Solidi B **241**, 1945 (2004).
[23] V. B. Mikhailik, H. Kraus, G. Miller, M. S. Mykhaylyk, and D. Wahl, J. Appl. Phys. **97**, 083523 (2005).
[24] S. Rajagopal, D. Nataraj, O. Yu. Khyzhun, Yahia Djaoued, J. Robichaud, and D. Mangalaraj, J. Alloys Compd. **493**, 340 (2010).
[25] Y. B. Abraham, N. A. W. Holzwarth, R. T. Williams, G. E. Matthews, and A. R. Tackett, Phys. Rev. B **64**, 245109 (2001).
[26] J. Li, Z. Chen, X. X. Wang, and D. M. Proserpio, J. Alloys Compd. **28**, 262 (1997).
[27] T. You, G. X. Cao, X. Y. Song, C. H. Fan, W. Zhao, Z. L. Yin, and S. X. Sun, Mater Lett. **62**, 1169 (2008).
[28] B. H. Brandow, Adv. Phys. **26**, 715 (1977).
[29] R. Bharati and R. A. Singh, J. Mater. Sci. **16**, 775 (1981).
[30] J. S. Griffith, *The Theory of Transition Metal Ions* (Cambridge Press, London, 1961).
[31] S. Rajagopal, V. L. Bekenev, D. Nataraj, D. Mangalaraj, and O. Yu. Khyzhun, J. Alloys Compd. **496**, 61 (2010).
[32] M. Bacci, S. Porcinai, E. Mihóková, M. Nikl, and K. Polák, Phys. Rev. B **64**, 104302 (2001).
[33] V. V. Laguta, A. Vedda, D. Di Martino, M. Martini, M. Nikl, E. Mihóková, J. Rosa, and Y. Usuki, Phys. Rev. B **71**, 235108 (2005).
[34] I. Y. Kushnirenko, Z. T. Moroz, L. L. Nagornaya, S. G. Nedeiko, A. I. Stetsun, and I. A. Tupitsyna, J. Appl. Spectrosc. **56**, 160 (1992).
[35] Y. A. Hizhnyi, T. N. Nikolaenko, and S. G. Nedilko, Phys. Status Solidi C **4**, 1217 (2007).
[36] M. Nikl, P. Bohäcek, K. Nitsch, E. Mihoková, M. Martini, A. Vedda, S. Croci, G. P. Pazzi, P. Fabeni, S. Baccaro *et al.*, Appl. Phys. Lett. **71**, 3756 (1997).
[37] K. V. Lamonova, E. S. Zhitlukhina, R. Y. Babkin, S. M. Orel, S. G. Ovchinnikov, and Y. G. Pashkevich, J. Phys. Chem. A **115**, 13596 (2011).